Electronic structure of β-$VOPO_4$

M. G. Willinger, D. S. Su, and R. Schlögl
Department of Inorganic Chemistry, Fritz-Haber-Institut der Max-Planck-Gesellschaft, Faradayweg 4-6, D-14195 Berlin, Germany
(Received 18 October 2004; published 26 April 2005)

Vanadium phosphorus oxides are used as catalysts in the selective oxidation of *n*-butane to maleic anhydride. The working catalyst comprises besides the main pyrophosphate phase in which the vanadium is in a 4+ oxidation state also a, predominantly preparation dependent, amount of different pentavalent vanadyl-orthophosphate phases. In order to elucidate the role of the pentavalent phases it is necessary to investigate them in detail. The present work reports the synthesis, characterization and a detailed investigation of the electronic structure of bulk β-$VOPO_4$ in company with simulated and experimental core-shell excitation spectra.

DOI: 10.1103/PhysRevB.71.155118 PACS number(s): 71.20.Be, 78.70.Dm, 79.20.Uv

I. INTRODUCTION

Vanadium phosphorus oxides (VPO) are a very complex and fascinating system characterized by an easy formation and inter conversion of several crystalline phases. VPO are commercially used as catalysts for the synthesis of maleic anhydride in the partial oxidation of *n*-butane. The phase constitution and the morphology of VPO catalysts are found to be dependent on the preparation routes and the applied solvent as well as on details of activation.[1] The final catalyst consists of the main V^{4+} phase $(VO)_2P_2O_7$ and a mixture of pentavalent phases.[2] These phases are crucial for the conversion and selectivity rate of the final catalyst. It is believed that only a specific combination of V^{4+} and V^{5+} phases leads to the high catalytic performance:[3] the presence of the crystalline V^{5+} phases in combination with the vanadyl pyrophosphate is thought to enhance the rate of oxidation of the adsorbed intermediates and cause a reduction of the self-inhibition effect and hence an improved catalytic behavior. Volta *et al.*[4] have explored the correlation between presence of $VOPO_4$ and catalytic behavior using a combination of various physico-chemical techniques and found that an increase in the selectivity to maleic anhydride, but a decrease in butane conversion can be related to the presence of α-$VOPO_4$ together with $(VO)_2P_2O_7$.

One way to get a more profound understanding of the real catalyst and the role of the different phases is to reduce the complexity of the system by investigating the specific occurring phases in depth on their own. Several different polymorph of the oxidized $VOPO_4$ have been reported in the literature:[5–8] α_I-$VOPO_4$, α_{II}-$VOPO_4$, β-$VOPO_4$, γ-$VOPO_4$, δ-$VOPO_4$, ϵ-$VOPO_4$, and ω-$VOPO_4$. During thermal treatment at high temperature the consecutive transitions $\alpha_I \rightarrow \alpha_{II} \rightarrow \beta$-$VOPO_4$ or $\delta \rightarrow \gamma \rightarrow \beta$-$VOPO_4$ have been observed.[5] β-$VOPO_4$ is considered to be the most stable phase among anhydrous orthophosphates. Schrader *et al.*[9,10] observed the conversion of β-$VOPO_4$ to $(VO)_2P_2O_7$ at 500°C in 2% *n*-butane/air. $(VO)_2P_2O_7$ can also be oxidized to β-$VOPO_4$ by means of O_2.[11]

This work is focused on the characterization of β-$VOPO_4$ by a combination of theoretical and experimental methods. *Ab initio* band structure calculations based on density functional theory (DFT) were performed in order to evaluate the bulk electronic structure. Core level spectroscopic methods were applied to experimentally probe the electronic structure at the ionized species: electron energy loss spectrometry (EELS) at the oxygen *K* ionization edge and near edge x-ray absorption spectroscopy (NEXAFS) at the V *K* ionization edge. The gained spectra are interpreted by means of the calculated band structure and compared to simulated spectra.

II. GEOMETRIC STRUCTURE

The structure of β-$VOPO_4$ consists of PO_4 tetrahedra and irregular VO_6 double pyramids. The double pyramids are linked along the *a* direction by sharing a common apex. They form a zigzag-like chain in which the pyramid axis are alternately tilted by ±20.8° toward the *c* direction (see Fig. 1). Within a double pyramid, the vanadium atom is shifted from the center of the square plane toward the vanadyl oxygen (see Fig. 2). The singly coordinated vanadyl oxygen (O4) defines the pyramid axes by a short V=O double bond of 1.57 Å and an additional, faint interaction with the vanadium atom of the next pyramid at a distance of 2.59 Å. Three structurally different oxygens (O1–O3) define the four equatorial corners of the double pyramid: O1 defines the two corners in the *y* direction, O2 and O3 define the corners in the *x* direction. The resulting distorted geometry of the pyramids is typical for vanadium in an oxidation state of +5 or +4.[12] Chains of VO_6 units are separated from each other by PO_4 tetrahedra which are linked to the oxygens of the equatorial plane. Each PO_4 tetrahedron spans the space between three neighboring chains of double pyramids by sharing two corners (O2, O3) with two subsequent double pyramids of one chain and two corners ($2\times$O1) with the adjacent chains in the $+b$ and $-b$ directions, respectively. The primitive cell comprises four formula units.

III. SYNTHESIS AND CHARACTERIZATION

Due to the easy transformation between the different $VOPO_4$ polymorph and the close agreement in their synthesis procedure, the preparation has to be done very carefully.

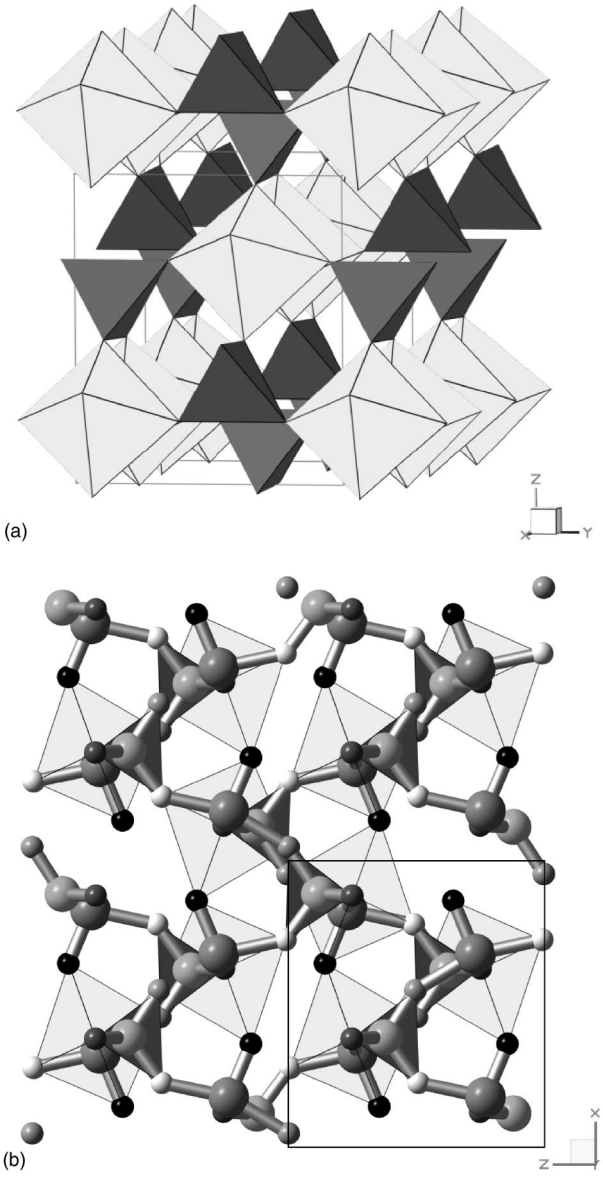

FIG. 1. Crystal structure of β-$VOPO_4$, viewed from [100] direction in (a) and from [010] direction (b). The orthorhombic unit cells are indicated; a, b, and c are parallel to x, y, and z axis, respectively. Four structurally different oxygens are present: vanadyl oxygen (O4, black) is bond only to vanadium, bridging oxygens (O1, dark gray, O2, white and O3, gray) are shared between vanadium and phosphorus. For clarity, groups of atoms are combined to VO_6 octahedra and PO_4 tetrahedra.

β-$VOPO_4$ was synthesized by oxydehydration of $VOHPO_4 \cdot 0.5H_2O$ at 680°C for 4 h under dry oxygen. In order to check the phase purity of the synthesized product, a combination of characterization methods were applied: scanning electron microscopy (SEM) and energy dispersive x-ray detection (EDX) to investigate the morphology and the atomic ratio, respectively; x-ray diffraction (XRD) for phase analysis and high resolution transmission electron microscopy (HRTEM) for microstructural analysis. The following instruments have been used: SEM and EDX were performed with a Hitachi S-4000 SEM, XRD spectra were recorded

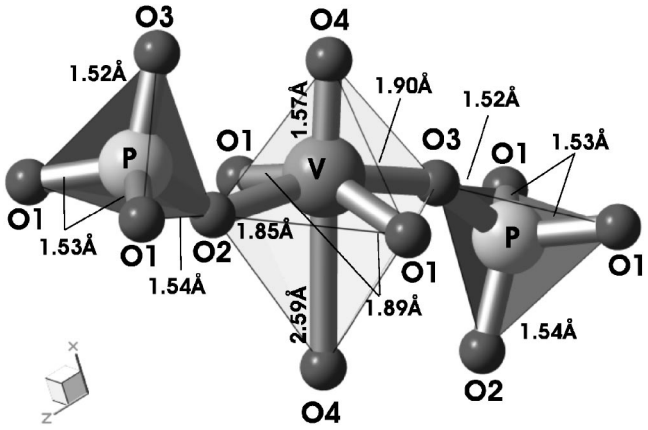

FIG. 2. Arrangement and bonding distances of the different oxygens in β-$VOPO_4$.

with a Stoe Powder Diffractometer with a position sensitive detector and HRTEM investigations have been performed with a Philips CM 200 field emission transmission electron microscope.

The SEM investigation reveals that β-$VOPO_4$ is composed of irregular shaped particles of a size varying from 0.5 to 2 μm (see Fig. 3). The measured atomic ratios are consistent with the stoichiometry of β-$VOPO_4$. XRD measurements obtained using Cu K_α radiation in the angular range (2θ) of 15 to 75° show a good agreement with the simulated (POWDERCELL software[13]) x-ray diffraction diagram in both positions and intensities of the peaks (see Fig. 4). No unassigned peaks are visible in the recorded angular range. Due to the likely existence of small portions of phases which are below the detection limit of XRD it can only be stated that the synthesized product is at least "XRD pure." Changes during the recording process due to x-ray irradiation could not be observed. The crystallinity of β-$VOPO_4$ is observed in lattice fringe images obtained by HRTEM as shown in Fig. 5. However, amorphous parts were observed to appear during high dose electron irradiation.

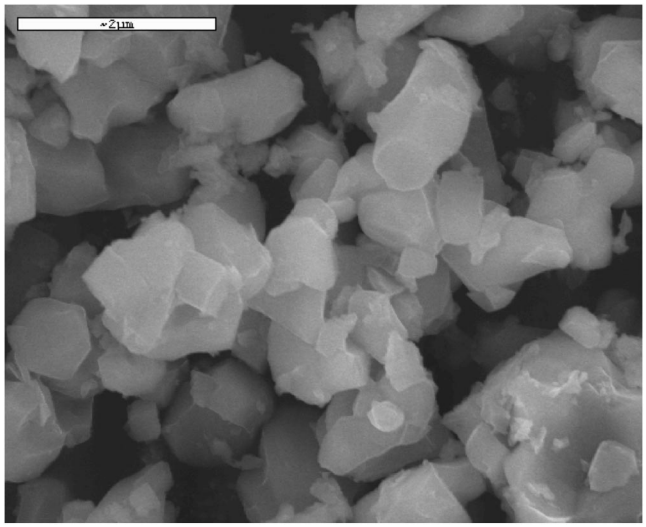

FIG. 3. SEM image showing irregular shaped particles of β-$VOPO_4$.

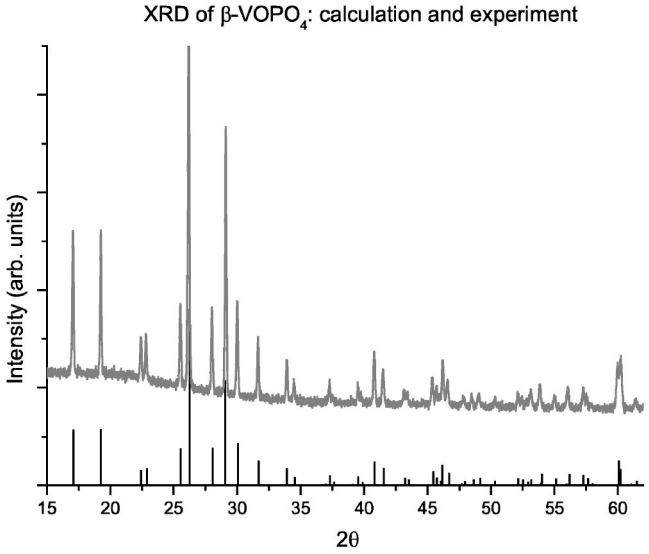

FIG. 4. XRD of β-$VOPO_4$. Calculated and experimental XRD spectra present a good agreement in both peak positions and intensities.

IV. CALCULATION AND EXPERIMENTS

Band-structure calculations of the density of states (DOS) were performed in the framework of density functional theory by using the full potential linear augmented plane waves code WIEN2K.[14] This package includes the TELNES program which allows to simulate electron energy loss spectra (EELS) by calculating the sum over site and angular-momentum projected DOS and DOS-cross terms multiplied by the appropriate transition matrix elements.[15] For the calculation a simple unit cell was used, and three-dimensional periodic boundary conditions ensure that the space-group symmetry is included properly. The calculation was performed with 80 k points in the irreducible part of the Brillouin zone and a plane wave cutoff parameter $R_{k\max}$ of 7.0 (corresponding to an energy cutoff of 28.7 Ry). The generalized gradient approximation (GGA) was used for the exchange-correlation potential.[16] The values of muffin-tin sphere radii were taken equal to 1.45 Bohr for V and P and 1.3 Bohr for O, respectively. In order to get a good basis set for the projection of the DOS onto p and d states in the simulation, the local coordinates at each atom of the tilted VO_5 pyramids were chosen such that the z axis coincides with the direction of the V=O vanadyl bond. This choice also determines the orientation of the local coordinates at the PO_4 tetrahedra except for the one oxygen that is shared with a VO_5 pyramid of different orientation.

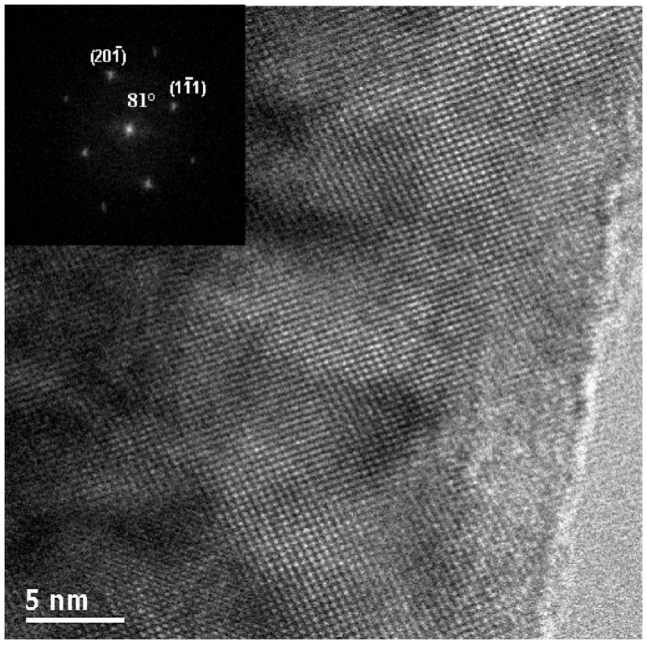

FIG. 5. HREM image of β-$VOPO_4$ in the [132] zone axis.

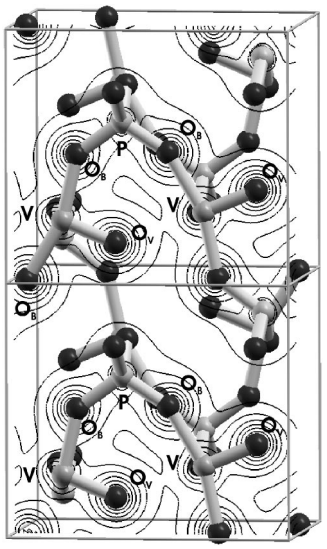

FIG. 6. Electron density contour plot given for a plane perpendicular to the b axis, passing through V-O-P and V=O bonds. Bridging and vanadyl oxygens are labeled as O_B and O_V, respectively. Isolines of electron density are given in the range between 0.1 and 8 e/Å^3 in a square root scale.

The EELS measurements were performed with a Philips CM 200 field emission transmission electron microscope equipped with a Gatan image filter for EELS measurements. The microscope was operated at 200 kV. The obtained energy resolution in the recorded spectra, estimated from the full-width at half maximum of the zero-loss peak, was 0.9 eV. The spectra were recorded at a spectrometer acceptance angle of β=9.8 mrad in order to average out any effects of anisotropy. The beam convergence angle was in the range of α=1.5 mrad.[17] Special care was taken in order to minimize irradiation effects. The NEXAFS of the V K edge was recorded at the Berlin electron synchrotron facility BESSY.

V. RESULTS AND DISCUSSION

A. Electron density

Figure 6 shows the electron density within a plane perpendicular to the b axis, chosen to intersect with vanadium centers and the bonds formed to bridging oxygens (V-O-P) and vanadyl oxygens (V=O). From the electron density dis-

tribution one can conclude that the bonds between vanadium centers and vanadyl oxygen exhibit more covalent than ionic bonding character, whereas in the case of bonds to bridging oxygens the situation is reversed. The electron density also reveals the reason for the characteristic difference between β-$VOPO_4$ and the layer structures of α_I-, α_{II}-, γ-, and δ-$VOPO_4$: In case of β-$VOPO_4$, the weak interaction between the vanadium center and the vanadyl oxygen belonging to the neighboring vanadium center (at a distance of 2.59 Å) is "bridged" by strong covalent bonded PO_4 units. They form a three-dimensional network by linking two oxygens of two subsequent VO_5 pyramids. In the layer compounds, PO_4 units connect four VO_5 pyramids within a plane, and the only interaction between planes is defined by the weak bond from the vanadium centers to the distant vanadyl oxygens of the next layer. The three dimensional network of β-$VOPO_4$ is the reason for its greater stability and the fact that the transformation from the layer $VOPO_4$ phases into β-$VOPO_4$ is irreversible. In view of catalysis, the greater stability might also explain the lower activity of β-$VOPO_4$ as compared to the layered $VOPO_4$ phases,[18] which offer a higher redox rate and higher rates of diffusion of oxygen into the bulk structure.

B. Density of states

1. Total DOS

The total DOS and the contributions of vanadium, oxygen, and phosphorus to the DOS in an energy region between −10 and 20 eV around the Fermi-level are presented in Fig. 7. Below the Fermi level the DOS consists of three blocks of bands. From a comparison of the different contributions follows that these bands mainly comprise oxygen states that are mixed with phosphorus states in the lower two sets of bands between −9 and −5 eV and with vanadium states in the energy range between −4.5 eV and the Fermi level. Above the Fermi level the DOS is dominated by vanadium states with only a small contribution from oxygen states in the lower conduction band between around 1.5 and 6 eV and by a combination of phosphorus and oxygen states in the upper conduction band above 8 eV.

2. Projected DOS

A deeper insight into the bonding relations and the hybridization of states is obtained form the angular momentum projected DOS at the vanadium, phosphorous, and oxygen sites, which are presented in Figs. 8–10. An inspection of the lower lying valence states reveals that bonding phosphorus *s* states are concentrated in the region between −9 and −7.5 eV followed by states of *p* character between −6.5 and −5 eV. Both form strong covalent σ bonds with 2*p* states from the surrounding oxygen atoms (O1, O2, and O3): the former with a_1 and the latter with t_2 symmetry. In contrast, the oxygen 2*p* states in the region between −4.5 eV and the Fermi-level form bonding combinations with states of V 3*d* character. The conduction band starts after a band gap of around 1.7 eV. The low lying conduction band between 1.7 and 6.2 eV originates mainly from V 3*d* states with only a small 2*p* contribution from oxygen. Due to crystal field effects the *d* band is split into three parts. This can be understood by considering the double pyramid as a distorted octahedron, in which the *z* axis coincides with the direction of the vanadyl bond. The V d_{xy} orbital is found well separated at the bottom of the *d* band and forms π^* combinations with the oxygen ligands of the pyramid base. The intermediate block, also

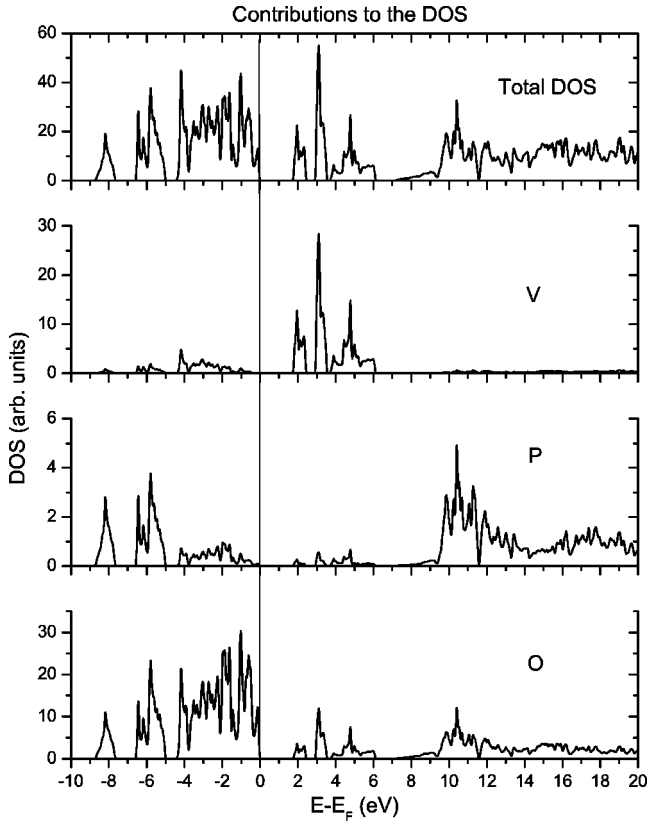

FIG. 7. Total DOS and the contributions of V, P, and O to the DOS of β-$VOPO_4$. Note the different scaling for the intensities in the diagrams.

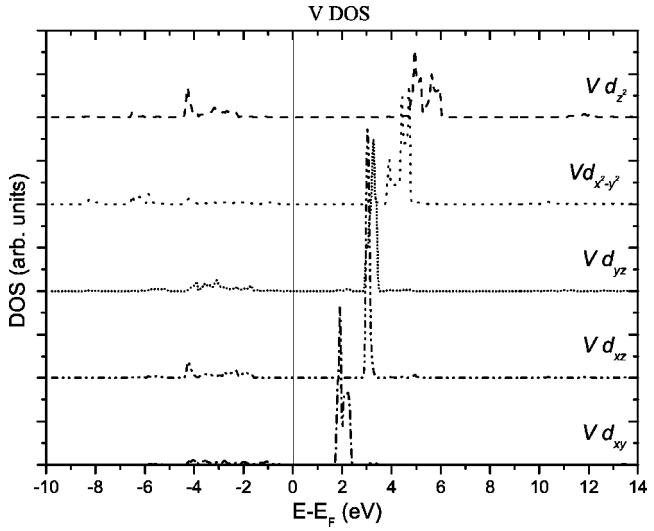

FIG. 8. V *d*-projected DOS.

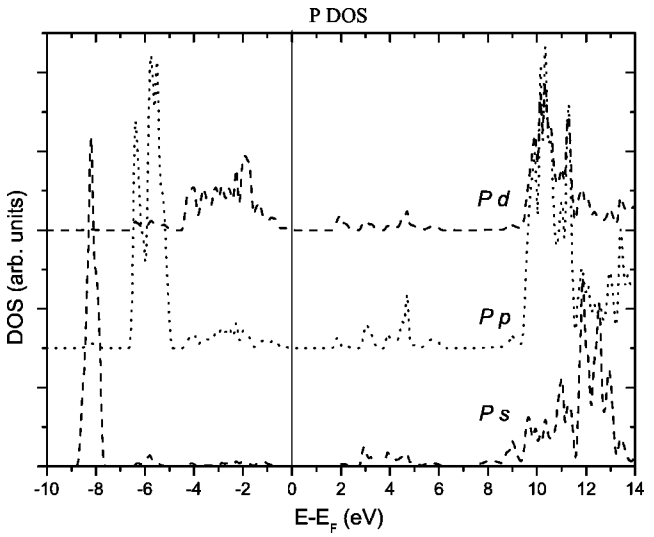

FIG. 9. P *s*, *p*, and *d* projected DOS.

corresponding to antibonding π^* states, is made up from d_{xz} and d_{yz} orbitals. They are slightly shifted to higher energies because of the small bonding distance to the vanadyl oxygen in *z* direction. Antibonding σ^* states are formed by $d_{x^2-y^2}$ and d_{z^2} orbitals at the top of the *d* band. After an additional band gap of around 1 eV the conduction band is dominated by antibonding combinations of oxygen 2*p* states with phosphorus 3σ states. The appearance of oxygen 2*p* character over the whole range of unoccupied states as well as the mixing of vanadium 3*d* states with oxygen 2*p* states in the valence band attests a covalent contribution to the bonding.

3. Differently coordinated oxygens

The existence of structurally different oxygens (see Fig. 2) becomes evident when the conduction band region of the different atom projected DOS are compared with each other. In the case of the vanadyl oxygen O4 the hybridization with vanadium 3*d* states leads to very localized antibonding π^* states at around 3 eV. These states are formed by a combi-

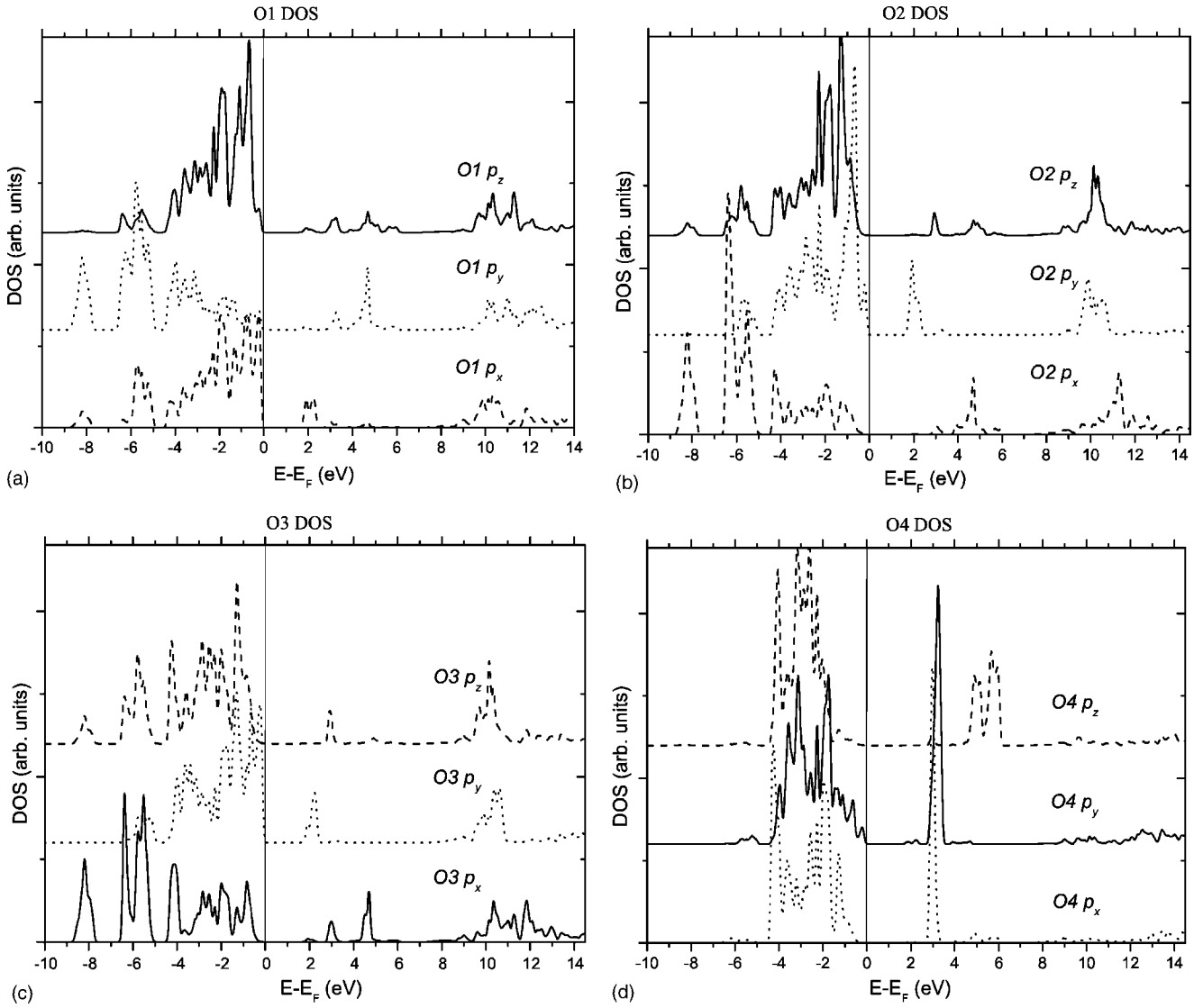

FIG. 10. O1, O2, O3, and O4 *p* projected DOS.

TABLE I. Summary of the main V $3d-$O $2p$ orbital overlap contributions.

	O1	O2	O3	O4
V $3d_{xy}$	$2p_x$	$2p_y$	$2p_y$	
V $3d_{xz}$		$2p_z$	$2p_z$	$2p_x$
V $3d_{yz}$	$2p_z$			$2p_y$
V $3d_{x^2-y^2}$	$2p_y$	$2p_x$	$2p_x$	
V $3d_{z^2}$				$2p_z$

nation of O4 $2p_x$ with V $3d_{xz}$ and O4 $2p_y$ with V $3d_{yz}$ orbitals, respectively. The remaining O4 $2p_z$ orbital contributes to a less localized σ^* combination with the V $3d_{z^2-r^2}$ orbital between 4.5 and 6.1 eV. The hybridization between these states is attested by the close agreement in the shapes of their projected DOS. Three structurally different oxygens set up the pyramid base. O1 makes up the two corners in the y direction of the base and forms π^* combinations with the V $3d_{xy}$ orbital and σ^* combinations along the y direction between its $2p_y$ orbital and the V $3d_{x^2-y^2}$ orbital. O2 and O3 define the corners of the pyramid basis in the x direction. Their $2p_y$ orbitals form π^* combinations with the V $3d_{xy}$ orbitals, while their $2p_x$ orbitals form σ^* combinations with V $3d_{x^2-y^2}$ orbitals. Due to the longer bond length between the V atom and the oxygen atoms of the pyramid base compared to the bonding distance of the vanadyl oxygen (O4), the splitting between bonding and antibonding combinations is lower for the former. This explains the fact that the π^* and σ^* combinations formed in the pyramid plane (i.e., d_xy and $d_{x^2-y^2}$) lie lower in energy than those formed with the vanadyl oxygen. Since the oxygen atoms of the pyramidal plane also form a bond to a phosphorus atom, their $2p$-projected DOS show intensities from antibonding and bonding combinations with the P $3\sigma^*$ states which are absent in the case of the vanadyl oxygen O4. An overview of overlapping orbitals is given in Table I.

C. O-*K* ELNES and V-*K* NEXAFS

EELS as well as NEXAFS were applied to probe the local electronic structure of oxygen and vanadium in β-$VOPO_4$, respectively. The shape of the vanadium and oxygen edges is strongly related to the oxidation state of the vanadium and to the distortion of the coordination polyhedra.[19]

EELS measurements were performed in the energy region of the V $L_{2,3}$ and the oxygen K ionization edges. A recorded spectrum is presented in Fig. 11 after background subtraction and multiple scattering correction.[20] The V $L_{2,3}$ ionization edges correspond to transitions from V $2p_{1/2}$ and $2p_{3/2}$ states to empty $3d$ states and show up as narrow peaks (white lines) at about 525.7 and 519 eV, respectively. From their position the oxidation state of vanadium can be estimated[21] as +5. While the fine structure of the O K ionization edge resembles the density of unoccupied states of p character, the shape and intensity of the V $L_{2,3}$ edges are strongly influenced by electron correlation effects. These effects are not accounted for within a one-electron approximation and therefore the simulation of their intensities fails. For this reason the following discussion is focused on the O K ionization edge.

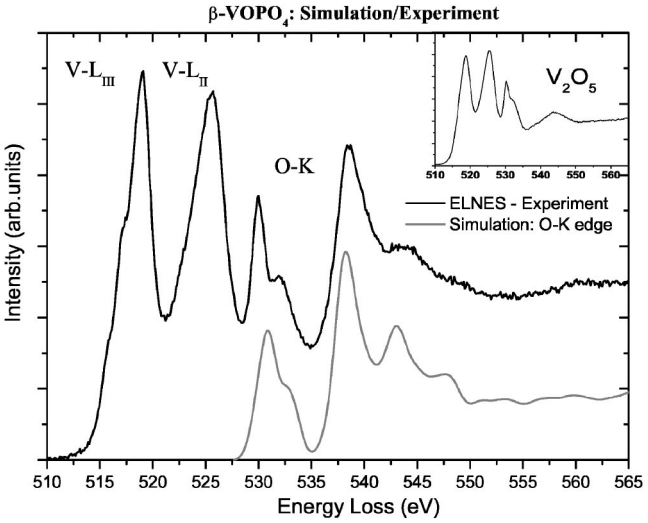

FIG. 11. EELS spectra of β-$VOPO_4$ and simulated oxygen K ionization edge (dotted line). For comparison, the spectrum of V_2O_5 is given in the upper right corner. The existence of distorted VO_5 pyramids in both compounds leads to the close agreement in the first region of the oxygen K edge.

Figure 11 shows the close agreement between simulation and experiment although the core hole left by the excited electron and the high-energy tail of the preceding V L_2 edge were not taken into account in the simulation. As already observed in the discussion of the DOS, the first empty states above the Fermi level are formed by a combination of unoccupied V $3d$ states with some admixture of O $2p$ character. The shape of the O K edge in the EELS spectrum between around 528 and 535 eV therefore resembles the electronic structure at the distorted VO_5 pyramid. This becomes evident when this region is compared to the spectra of V_2O_5 which consists of similarly distorted VO_5 pyramids (see inlay in Fig. 11). Two clearly developed peaks, separated by a ligand field splitting of approx. 2 eV reproduce transitions from a oxygen $1s$ state into unoccupied π^* and σ^* states, respectively. Above 535 eV another feature arises from transitions into unoccupied states formed by hybridization of O $2p$ and P 3σ states. A closer insight into the structure of the O K-edge is gained by splitting it into the contributions arising from the differently coordinated oxygens as shown in Fig. 12. This clearly demonstrates the role of the tightly bound vanadyl oxygen for the development of the first peak. The contributions from O2 and O3 are very alike, reflecting the close agreement in their surrounding. O1 contributes with a higher weight to the spectrum since it occupies two equivalent positions in each VO_5 pyramid.

The V K ionization edge NEXAFS is presented in Fig. 13. A narrow pre-edge peak is observed in front of the main edge. It arises mainly from dipole transitions to the lowest empty states localized at the coordination polyhedron of vanadium. As already discussed, these states are mainly made up from vanadium $3d$ atomic orbitals. Transitions into these final states occur only because of the nonzero p component relative to the vanadium atom that is produced by the super-

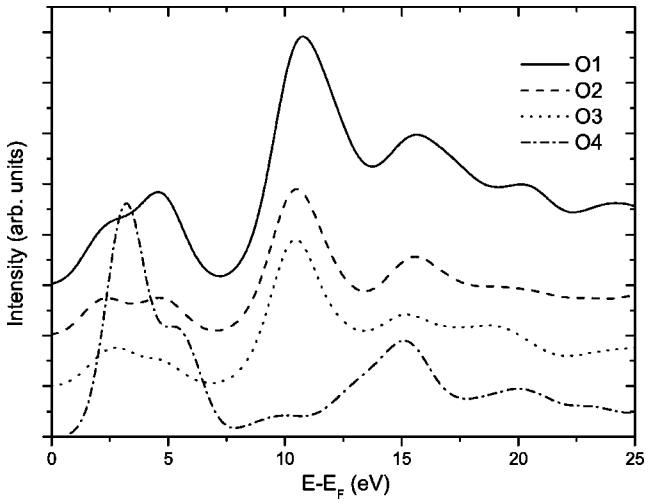

FIG. 12. Contributions of the different oxygens to the ELNES spectra of β-$VOPO_4$.

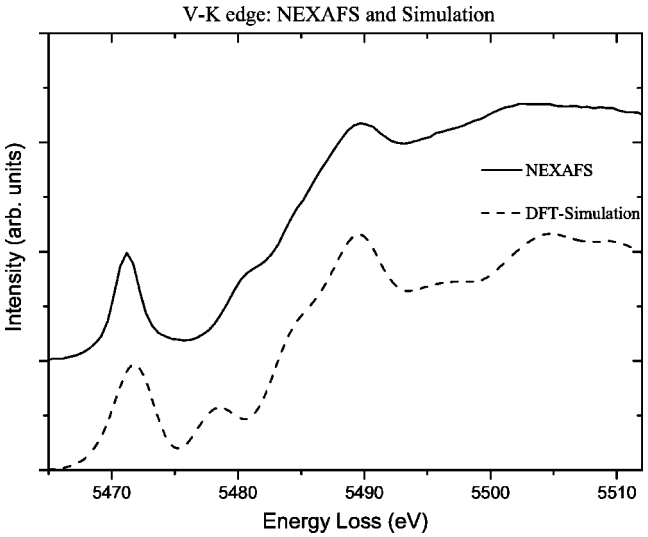

FIG. 13. β-$VOPO_4$: Vanadium *K* edge: NEXAFS experiment and DFT simulation (dotted line). Note that the energy scale of the simulated spectra was stretched by a factor of 1.2 (see text for more details).

position of the neighboring oxygen atom *p* orbitals due to the *p-d* mixing. Comparison with the simulated spectrum shows a good agreement although the energy scale in the simulation had to be stretched in order to account for self-energy effects. These effects, which are a consequence of the chosen exchange-correlation functional, are larger for the V *K* edge than for the O *K* edge and it is well known that generalized gradient ("GGA") functionals include unphysical electron self-interactions which lead to an energy-dependent compression of the energy axis in the simulated spectra.[22,23]

D. Conclusion

In the field of VPO systems with its huge variety of phases it is of importance to elucidate the electronic structure of the possible phases in a systematic way. It is a key issue in view of the high scientific interest focused on the family of VPO compounds from a variety of fields. Not only in view of catalysis, where the knowledge of the electronic structure of β-$VOPO_4$ helps to understand and follow possible transformations between different phases of working VPO catalysts, but also in the field of materials science, where Li intercalated VPO is used as cathode material for rechargeable batteries, a systematic investigation of the underlying VPO phases is of high priority. In this work, the electronic structure of β-$VOPO_4$ has been determined in terms of electron density and density of states and used for the simulation of core excitation spectra. The electron density distribution reveals how corner sharing of VO_5 pyramids and strongly bonded PO_4 units forms a three-dimensional network which is responsible for the higher stability of β-$VOPO_4$ with respect to the layered $VOPO_4$ phases. A detailed insight into bonding properties such as hybridization and covalent versus ionic bonding was gained from an inspection of the site and angular momentum projected density of states. The view of chemically independent PO_4 and VO_5 building blocks is therefore justified by the fact that contributions to the density of states are well separated in energy for different bonds. The electronic structure is thus most sensitive to the local surrounding of the vanadium atoms and the geometry of the PO_4 tetrahedra, but less sensitive to the orientation of the PO_4 units with respect to the V-O-P bonding axis, which finally determines how the three-dimensional structure is set up. In a following paper, the electronic structure of α_{I}-, α_{II}-, and β-$VOPO_4$ will be compared to each other with a focus on this aspect. Preliminary results demonstrate the small effect of differently oriented PO_4 linking units on the electronic structure of $VOPO_4$ phases with consist of corner shared structural units. Simulated core excitation spectra are in very close agreement with the experimental spectra, although simulations were based on ground-state DFT calculations. This offers the possibility of tracing back structural features present in recorded spectra to the underlying transitions at the corresponding sites. Spectral features are hence well understood and can be used to interpret spectra from VPO samples of unknown phase composition as well as changes observed during experiments such as *in situ* XAS.

ACKNOWLEDGMENTS

This work is supported by the SFB 546 of the Deutsche Forschungsgemeinschaft. The author would like to thank J. B. Wagner for helpful discussions.

[1] G. J. Hutchings, C. J. Kiely, M. T. Sananes-Schulz, A. Burrows, and J.-C. Volta, Catal. Today **40**, 273 (1998).
[2] F. J. C. Sanchez, J. A. Lopez-Sanchez, R. P. Wells, C. Rhodes, A.-Z. Isfahani, and G. Hutchings, Catal. Lett. **77**, 189 (2001).
[3] C. J. Kiley, A. Burrows, S. Sajip, G. J. Hutchings, M. T. Sananes, A. Tuel, and J.-C. Volta, J. Catal. **162**, 31 (1996).
[4] N. H. Batis, H. Batis, A. Ghorbel, J. C. Vendrine, and J.-C. Volta, J. Catal. **128**, 248 (1991).
[5] E. Bordes, Catal. Today **1**, 499 (1987).
[6] F. B. Abdelouahab, N. G. R. Olier, F. Lefebvre, and J.-C. Volta, Appl. Catal., A, **157**, 173 (1997).
[7] B. Jordan and C. Calvo, Can. J. Chem. **51**, 2621 (1973).
[8] P. Amorós, M. D. Marcos, M. Roca, J. Alamo, A. Beltrán-Porter, and D. Beltrán-Porter, J. Phys. Chem. Solids **62**, 1393 (2001).
[9] T. P. Moser and G. L. Schrader, J. Catal. **104**, 99 (1987).
[10] *New Developments in Selective Oxidation*, edited by M. E. Lashier, T. P. Moser, and G. L. Schrader (Elsevier Science Publishers, Amsterdam, 1990).
[11] M. E. Lashier and G. L. Schrader, J. Catal. **128**, 113 (1991).
[12] C. Hébert, M. Willinger, D. S. Su, P. Pongratz, P. Schattschneider, and R. Schlögl, Eur. Phys. J. B **28**, 407 (2002).
[13] W. Kraus and G. Nolze, *POWDERCELL for Windows Version 2.3*, 1999.
[14] WIEN2K, An Augmented Plane Wave + Local Orbitals Program for Calculating Crystal Properties, Techn. Universität Wien, Austria, 2001.
[15] C. Hébert-Souche, P.-H. Louf, P. Blaha, M. Nelhiebel, J. Luitz, P. Schattschneider, K. Schwarz, and B. Jouffrey, Ultramicroscopy **83**, 9 (2000).
[16] J. P. Perdew, K. Burke, and M. Ernzerhof, Phys. Rev. Lett. **77**, 3865 (1996).
[17] D. Su, C. Hébert-Souche, M. Willinger, and R. Schlögl, Micron **34**, 227 (2003).
[18] C. Srilaxmi, N. Lingaiah, A. Hussain, P. S. S. Prasad, K. V. Narayana, A. Martin, and B. Lücke, Catal. Commun. **5**, 199 (2004).
[19] D. S. Su, M. Wieske, E. Beckmann, A. Blume, G. Mestl, and R. Schlögl, Catal. Lett. **75**, 81 (2001).
[20] R. F. Egerton, *Electron Energy-Loss Spectroscopy in the Electron Microscope* (Plenum Press, New York, 1996).
[21] M. Willinger, Master's thesis, Vienna University of Technology, 2001.
[22] J. P. Perdew and A. Zunger, Phys. Rev. B **23**, 5048 (1981).
[23] J. J. Rehr and R. C. Albers, Rev. Mod. Phys. **72**, 621 (2000).